Co inside hollow carbon spheres (HCSs) as an FT catalyst: spillover effects from Ru placed inside and outside the HCS

Tumelo N. Phaahlamohlaka,[a,c] Mbongiseni W. Dlamini,[a,c] David O. Kumi,[a] Roy Forbes,[a] Linda L. Jewell,[b,c] , Neil J. Coville*[a,c,]

[a]Molecular Sciences Institute, School of Chemistry, University of the Witwatersrand, Johannesburg 2050, South Africa.

[b]Department of Chemical Engineering, University of South Africa, Private Bag X6, Florida, 1710, South Africa.

[c]DSI-NRF Centre of Excellence in Catalysis (c*change)

[d]DSI-NRF Centre of Excellence in Strong Materials

Graphical abstract

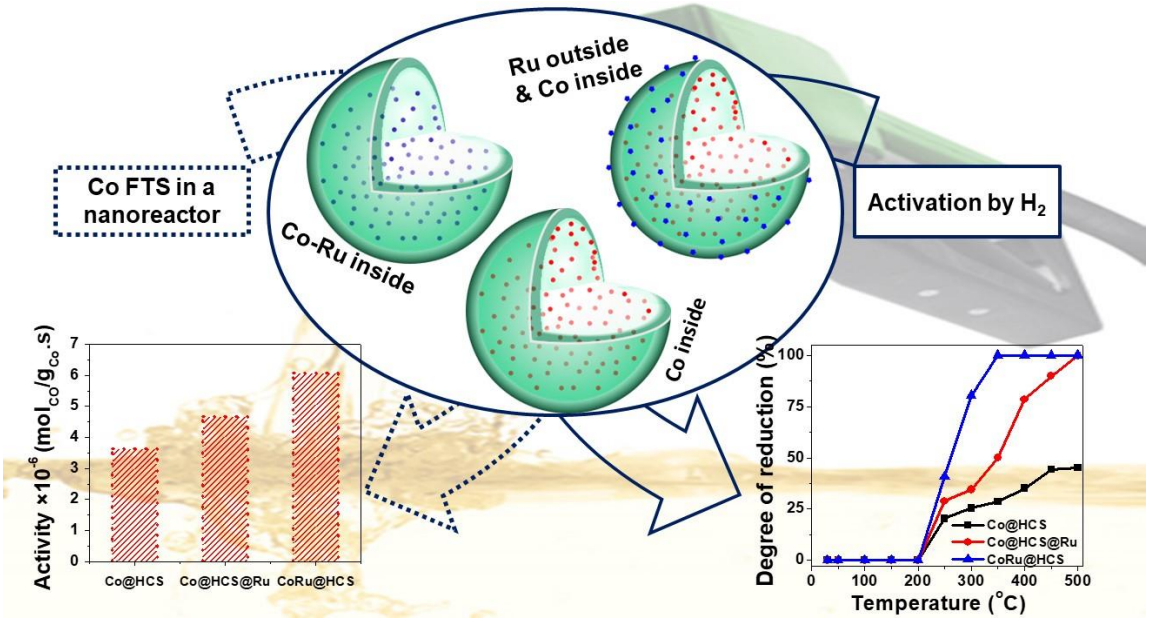

Abstract: Hollow carbon spheres (HCS) containing Co nanoparticles placed inside the HCS were synthesized for the first time using polystyrene spheres as a template. The encapsulated Co nanoparticles, after reduction, showed Fischer-Tropsch (FT) activity indicating syngas accessibility through the HCS porous shell. Two Co catalysts promoted by Ru, placed either inside or outside the HCS (CoRu@HCS and Co@HCS@Ru), were also synthesized and

characterized. The location of the Co and Ru was confirmed by SEM and TEM analyses. In-situ XRD studies indicated enhanced H_2 reduction of the Co oxide to Co, inside the HCS, in the order CoRu@HCS >Co@HCS@Ru > Co@HCS. The CoRu@HCS catalyst had the highest FT activity, and this was ascribed to a primary spillover effect associated with the direct contact of the Co and Ru inside the HCS. A small secondary spillover effect was also noted for Co@HCS@Ru.

Keywords: Metal encapsulation; Cobalt; Hollow carbon spheres; Fischer-Tropsch; Metal reduction ; Ruthenium; Spillover

1. Introduction

The synthesis of metal nanoparticles encapsulated inside hollow porous spheres has attracted much attention over the years. This is because most of these composite materials have been shown to give novel properties that are applicable to many scientific disciplines **[1-3]**. The hollow porous spheres have typically been prepared using different materials such as silica, titania, and carbon **[4-6].** The synthesis of hollow carbon spheres (HCSs) has been achieved by employing two generic approaches using a soft template or a hard template. In both methods, the template is covered by a carbon layer and removal of the template produces the HCS **[7]**.

Two general methods can be used to load a metal, M, into an HCS, to make M@HCS materials. The first is to create the HCS and then introduce the metal into the HCS **[2, 8]**. Another procedure, commonly used, is to add M to the template surface, cover the surface with carbon and then remove the template, leaving the metal behind inside the HCS **[9]**. In many studies, modified or unmodified Stöber silica spheres have been used as the template to successfully encapsulate noble metal nanoparticles such as Pt **[10]**, Au **[11]**, Pd **[12]**, and Rh **[13]** inside porous hollow carbon spheres.

However, this approach does not work for all metals, as removal of the SiO_2 template can also result in the removal of metal M. Thus, our initial attempts to make Co@HCS using SiO_2 were unsuccessful as the base or the HF used to remove the SiO_2, also removed the Co.

To overcome this issue, templates other than SiO_2 are needed. An alternative template that has been found to be useful in making HCSs is polystyrene **[14]**.

Polystyrene spheres (PSSs) provide an alternative to SiO_2 for use as a hard template in the synthesis of hollow carbon spheres **[10-13]**. They can be synthesized easily on a large scale by well-known procedures **[15]**. Polystyrene spheres offer a softer template when compared to silica spheres because the removal of the polystyrene template, after carbon coating, does not require harsh conditions (i.e. the use of HF). The polystyrene template spheres can easily be removed by solvents or by using a solventless method which involves heat treatment at ca. 400 °C under an inert environment using nitrogen or argon gases **[7, 14]**. For example, White et al. **[14]** managed to produce well-dispersed hollow carbon spheres by coating polystyrene spheres with glucose using a hydrothermal method and then by thermal removal of the PSSs, hollow carbon spheres with good porosity and high BET surface area > 350 $m^2.g^{-1}$ could be obtained after annealing and carbonization.

In this study, a method is presented to encapsulate Co (and CoRu) nanoparticles inside hollow carbon spheres. This study represents the first example of a process for placing Co inside a HCS and provides a unique catalyst for studying the Fischer-Tropsch (FT) reaction. In a previous study we were able to make a HCS in which the Co was placed outside the HCS and similarities and differences with this study will be highlighted.

The process to make Co@HCS entailed the synthesis of PSSs which were then covered by a mesoporous carbon layer and after removal of the PSS yielded a mesoporous HCS (HCS). Addition of either Co, or Co and Ru, to the PSSs yielded Co/PSS and CoRu/PSS which were then coated with a mesoporous carbon shell followed by thermal removal of the PSSs to give the Co@HCS, and CoRu@HCS catalysts. The addition of Ru to the Co@HCS readily gave Co@HCS@Ru.

These three catalysts (Co@HCS, CoRu@HCS and Co@HCS@Ru) were synthesized to study the both the effect of placing Co inside a HCS and the effect of Ru promotion on Co nanoparticles when separated by the HCS carbon layer. In many reactions the promotion of catalysts is carried out to enhance both the activity and selectivity of the catalyst. For example, in the Fischer-Tropsch reaction, Co is promoted by a range of noble metals

including Ru **[16-18]**. One of the processes by which the Ru affects the Co catalyst is believed to be spillover in which H atoms spillover from the Ru to the Co to aid in the Co reduction **[17]**. An issue of importance relates to the ability of the spillover hydrogen to travel from the Ru to the Co. When the promoter and metal are in contact this is called primary (intimate) spillover and when they are separated this is called a secondary hydrogen spillover **[19-22]**. Studies on the use of reducible metal oxide supports have clearly shown that secondary hydrogen spillover can occur over TiO_2 supports **[21].** The issue is less clear cut on carbon supports where defects may play an important role **[23]**.

In this study, we have made use of the HCSs to provide a defined barrier between the Co and the Ru to allow for the investigation of both primary and secondary spillover effects. This study is similar to a study in which we placed the Co outside the HCS and the promoter (Ru) inside HCS **[18]** and in this case the complete separation between the Co and Ru in Co@HCS@Ru is also guaranteed. In this study, by placing the Co inside the HCS, we have also been able to test the concept of the nanoreactor in FT catalysis. All the Co atoms are contained in HCSs and each HCS acts as a small reactor (d < 400 nm) and the effect of this encapsulation process has been explored.

2. Experimental procedure

2.1. Chemicals

Styrene (Aldrich), polyvinylpyrollidone (PVP, MW 40 k, Aldrich), cobalt nitrate hexahydrate (Aldrich), ethylene glycol (Aldrich), ammonia solution (25%; Fluka), potassium persulfate (Eimer and Amend), hexadecyltrimethylammonium bromide (CTAB; Aldrich), ruthenium chloride (Aldrich), hydrazine (35%, Aldrich), ethanol (98%; Merck), isopropanol (99%, Merck), nitric acid (55%; Merck), hydrochloric acid (32%, Associated chemical) were used as received. Deionized water was used in all the experiments where water was used.

2.2. Synthesis of polystyrene spheres (PSSs) [15]

Styrene (8 mL) and PVP (0.1 g) were dispersed and dissolved respectively in 250 mL of a water-ethanol mixture (water, 200 mL and ethanol 50 mL) by sonication and then stirred for 15 min. A potassium persulfate solution (0.15 g in 20 mL water) was added to this solution

while stirring. The mixture was then heated at 80 ℃ for 27 hours. After cooling the product was then filtered and washed repeatedly using water.

2.3. Loading of Co or CoRu on the polystyrene spheres (3%Co/PSSs or 3 %Co 0.2%Ru/PSSs)

PSSs (6 g) were dispersed by sonication for 30 minutes in a 200 mL water/ethanol solution (150 mL and 50 mL respectively). To this solution was added cobalt nitrate hexahydrate (0.89 g) while stirring until it completely dissolved to form a red solution. Deposition of Co nanoparticles was performed by the slow addition of a hydrazine solution (20 mL, 2 M) to the Co containing solution. The solution was left stirring for 12 hours to ensure complete deposition of the Co nanoparticles. To make the bimetallic CoRu/PSSs composite the cobalt precursor and a $RuCl_3$ solution (11.9 mL, 0.01 M) were added together before nanoparticle precipitation. The nominal loading was calculated to be 3% Co and 0.2% Ru.

2.4. Synthesis of Co or CoRu nanoparticles inside hollow carbon spheres

PSSs, CoRu/PSSs or Co/PSSs (6 g) and ammonia solution (25%; 4.5 mL) were dispersed by sonication for 30 min in 450 mL of an ethanol/water solution (300 mL ethanol and 150 mL water). A resorcinol (2.25 g), formaldehyde solution (37%; 4.5 mL) and CTAB (3 g) mixture made in ethanol (150 mL), was then added to the PSSs, Co/PSSs or CoRu/PSSs mixture which was then stirred at room temperature for 20 h to form a resorcinol-formaldehyde (RF) polymer around the PSSs, CoRu/PSSs or Co/PSSs. The resulting composite (PSS@RF, CoRu/PSSs@RF or Co/PSSs@RF was then filtered and washed repeatedly with water followed by drying at 80 ℃ for 12 hours. Template removal and carbonization was performed following a one-step procedure inside a horizontal quartz tube by heating CoRu/PSSs@RF or Co/PSSs@RF under a nitrogen flow (50 mL/min) at 350 ℃ for 1 hour to decompose and remove the polystyrene template. This was followed by annealing of the carbon spheres at 600 ℃ for 2 hours under a nitrogen atmosphere. The resulting products were called HCS, Co@HCS and CoRu@HCS (HCS = porous hollow carbon spheres)

2.5. Preparation of Co@HCS@Ru

Synthesis of Ru nanoparticles **[24]**

Ruthenium chloride solution (20 mL, 0.01 M) was added to ethylene glycol (15 mL) in a round bottomed flask. PVP (0.1 g) was added to this solution while stirring to ensure that it dissolved. The Ru nanoparticle synthesis was performed by reduction of the Ru ions using ethylene glycol under reflux at 200 ℃ for 6 hours. The resulting nanoparticles were precipitated using isopropanol and recovered by centrifugation at 15 000 rpm while washing with ethanol to remove all the ethylene glycol. The clean nanoparticles were dispersed in ethanol (50 mL) and stored at room temperature.

Loading of Ru nanoparticles on Co@HCS

The Co@HCS (1.5 g) catalyst was dispersed in 50 mL ethanol followed by the addition of the dispersed Ru nanoparticles (30 mL). This mixture was sonicated for 30 minutes and then stirred for 12 hours to load the Ru nanoparticles. The catalyst was filtered and washed using ethanol followed by drying at 100 ℃ overnight.

All the catalysts (Co@HCS, CoRu@HCS, Co@HCS@Ru) were calcined at 210 ℃ under 5% O_2/Ar (50 mL/min) for a further 2 hours to ensure that all the cobalt was converted to the Co_3O_4 phase.

2.6. Material characterization

TEM analysis was performed on a Tecnai spirit (T12) transmission electron microscope operating at 120 kV. The samples were dispersed in methanol by ultrasonication and loaded onto a copper grid for TEM analysis. The particle size distribution of the materials formed was determined by counting at least 200 randomly selected particles per sample from different TEM images. Gaussian statistics yielded values for the average particle sizes. SEM analysis was performed on a FEI Nova Nanolab 600 FIB/SEM instrument operating at 30 kV. The samples mounted on a carbon tape were coated with a gold-palladium layer before the analysis. The bulk composition of the catalysts was analyzed using a Bruker D2 phaser equipped with a Lynxeye detector, using a Co-Kα (λ = 0.17889 nm) at 30 kV. The scan ranged from $10° < 2\theta < 90°$ in 0.0260° steps.

TGA was performed with a Perkin- Elmer STA6000 TGA using nitrogen or air as the purge gas and a heating rate of 10 ℃.min^{-1}. The flow rate of the purge gas was always 20 mL.min^{-1}. N_2 adsorption–desorption experiments were conducted at -195 ℃ using a Micromeritics Tristar 3000 surface area and porosity analyzer. Prior to each experiment, the sample was outgassed at 150 ℃ for 4 hours under N_2 gas. The BET surface areas were obtained from adsorption data in a relative pressure range from 0.05 to 0.30. The total pore volumes were calculated from the amount of N_2 vapor adsorbed at a relative pressure of 0.99. The pore size distributions were evaluated from the desorption branches of the isotherms using the Barrett–Joyner–Halenda (BJH) method **[25, 26]**. The micropore surface area and volume were calculated using the t-plot report data. TPR experiments were carried out with a Micromeritics Auto Chem II unit. The catalyst (approximately 50 mg) was placed in a quartz tubular reactor, fitted with a thermocouple for continuous temperature measurement. The reactor was heated in a furnace. Prior to the temperature-programmed reduction measurement, the calcined catalysts were flushed with high-purity argon at 200 ℃ for 30 minutes, to remove water or impurities, followed by cooling to ambient temperature. Then, 5% H_2/Ar was switched on, and the temperature was raised at a rate of 10 ℃.min^{-1} from 50 to 850 ℃. The gas flow rate through the reactor was controlled by three Brooks mass flow controllers and was always 50 mL.min^{-1}. The H_2 consumption (TCD signal) was recorded automatically by a computer.

Pulse chemisorption was performed using the Micromeritics Auto Chem II instrument, to compute the number of active sites on the catalysts. The catalyst (ca. 100 mg) was placed in a quartz tubular reactor. The sample was reduced at 350 ℃ for 2 h under a hydrogen flow of 50 mL.min^{-1}. Before injecting the active gas, the sample was purged using helium gas at 350 ℃ for 1 h, followed by cooling to ambient conditions. Hydrogen chemisorption (assuming a H_2/Co ratio of 2) was then performed at 150 ℃ using ultra-pure hydrogen as the active gas and argon as the carrier gas.

The in situ PXRD experiments were performed on a Bruker D8 Avance fitted with an Anton Paar XRK 900 in situ cell. The diffractometer used a sealed copper tube as the X-ray source operating at 40 kV and 40 mA that provided X-rays with a wavelength of 0.15418 nm in a parallel beam geometry. Co loading on the HCSs was determined using an ICP-OES End on

Plasma from Spectro Genesis (Kleve, Germany). A catalyst sample (50 mg) was dispersed in a solution of 10 mL of 55% nitric acid and 40 mL water to dissolve the Co nanoparticles before analysis.

2.7. Fischer-Tropsch Synthesis.

The Fischer–Tropsch synthesis was performed in a fixed-bed micro-reactor. A gas cylinder containing a $H_2/CO/N_2$ mixture (~60/30/10 vol. % purity: 99.99) was used to supply the reactant gas stream to the catalyst with a flow rate of 15 $mL.min^{-1}$. N_2 was used as an internal standard in order to ensure accurate mass balances. Catalyst (1 g) was added to the reactor and reduced in situ at 250 ℃ for 2 hours under a stream of H_2 (1.5 bar at 50 $mL.min^{-1}$). After reduction, the reactor temperature was decreased to ambient temperature under a hydrogen flow, and then heated up to 220 ℃ under synthesis gas at a pressure of 10 bar. All gas lines after the reactor were kept at 100 ℃, and a hot trap placed immediately after the reactor was held at 150 ℃ in order to collect wax. A second trap kept at ambient temperature was used to collect the oil and water mixture. The flow was controlled using a metering valve and measured by a bubble meter. The product stream was analyzed online using two gas chromatographs. A thermal conductivity detector (TCD), equipped with a Porapak Q (1.50 m × 3 mm) packed column, was used to analyze H_2, N_2, CO and a flame ionization detector (FID), equipped with a Porapak Q packed column, was used for the analysis of the hydrocarbons online. Liquid and wax hydrocarbons collected in the knockout pots were analyzed using an offline GC, equipped with a ZB-1 packed column.

3. Results and Discussion

3.1. Catalyst Structure and Dispersion

The PSSs were made by a classical route with an average diameter = 359 nm (Figure S1a,e). The coverage of the PSS was performed with RF. The studies are similar to those reported by White et al. **[14]**, using a PSS template but in this study, resorcinol and formaldehyde were used as the carbon source instead of glucose. TGA studies of the PSS@RF showed clean removal of the PSSs to give HCS at ca. 420 ^oC (Figure S2a) with shell thickness = ca. 22 nm (Fig S2b).

The catalysts with encapsulated metal nanoparticles were made using the same procedure but with a prior step involving the addition of Co (and Ru) particles on the PSSs template before RF coating. The M@HCS, made from the RF followed by PSS removal all had a wall thickness of ca. 22 nm and diameters = 337 nm (Figure S1f). SEM images show the morphology of the materials after carbon coating of Co/PSSs (Figure S1b), and after RF coating and PSS removal to give Co@HCS and CoRu@HCS (Figure S1c,d). The monodisperse polystyrene spheres (PSSs) were readily coated (predominantly individually) with the resorcinol-formaldehyde (RF) as can be seen in Figure S1b. Resorcinol and formaldehyde have previously been effectively used to make hollow carbon spheres from Stöber silica sphere templates **[27, 28]** and it is clear that the polymerization of resorcinol and formaldehyde on the PSSs template followed a similar route to that on the SiO_2 spheres. Following the removal of the polystyrene template by heating in nitrogen, the resulting hollow carbon spheres took the shape of the template without any significant crumbling or breakage (Figure S1c, d).

TEM images, together with particle size distributions of the three catalysts [(a) Co@HCS (d_{Co3O4}, average size 7.4 nm), (c) CoRu@HCS (d_{Co3O4}, average size 7.1 nm) and (g) Co@HCS@Ru (d_{Co3O4}, average size = 7.3 nm) are shown in Figure 1. The presynthesized Ru nanoparticles are also shown in Figures 1(e) and (f) with their particle size distribution (d_{RuOx} size = 2.6 nm). The encapsulated Co_3O_4 nanoparticles were well dispersed inside the hollow carbon spheres. No cobalt oxide nanoparticles are expected to be found on the outside of the carbon shell using this procedure [1]. This procedure also ensures that the Ru nanoparticles are located on the outside and Co on the inside of the hollow carbon spheres and that there will be limited if any, contact between Co and Ru metal nanoparticles.

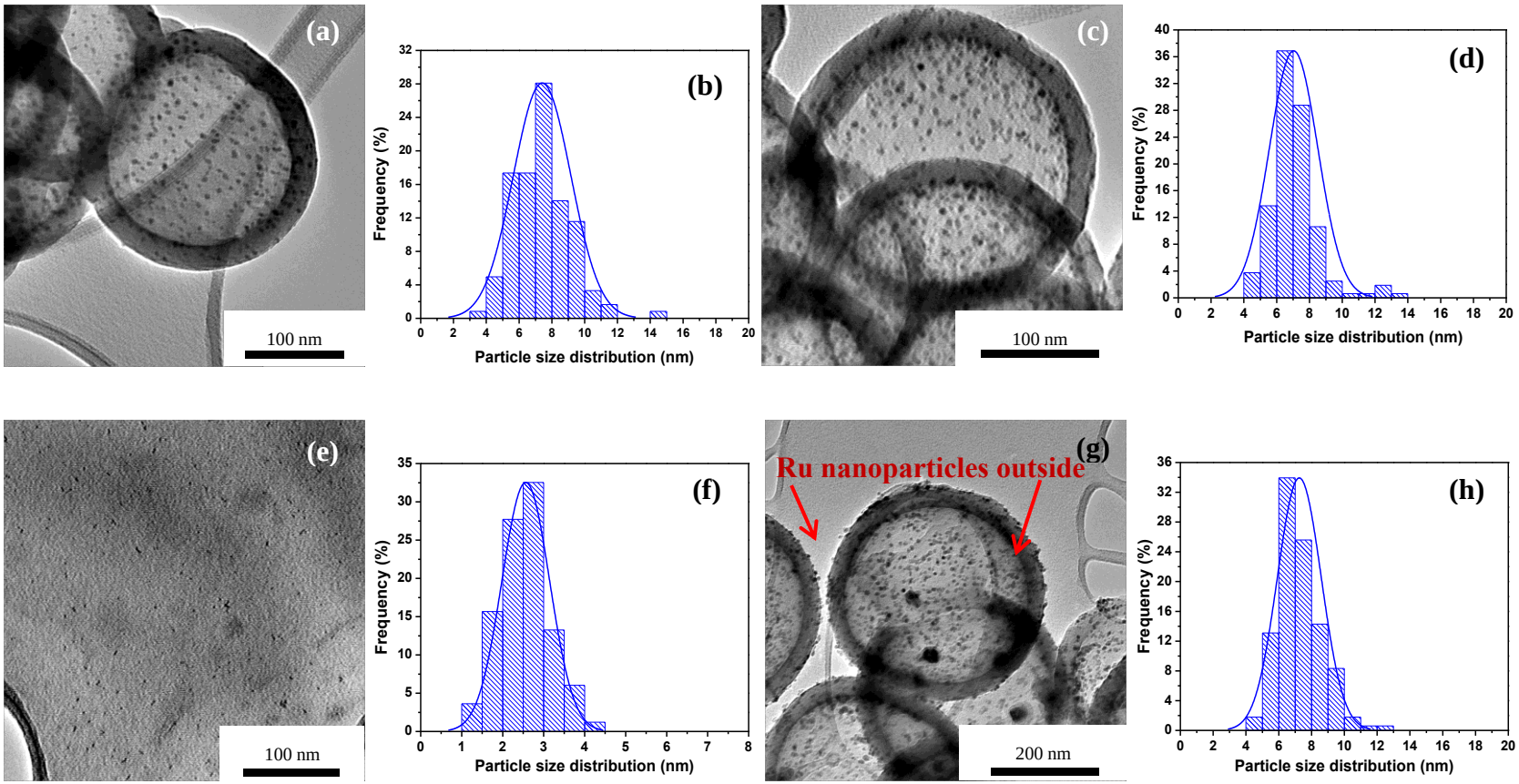

Figure 1: TEM images and particle size distribution of the prepared catalysts together with the pre-synthesized Ru nanoparticles. (a,b) Co@HCS (c,d) CoRu@HCS, (e,f) Ru nanoparticles, (g.h) Co@HCS@Ru

STEM analysis of the catalysts was also performed. A comparison of the STEM and SEM images indicates that the Co nanoparticles in CoRu@HCS (Figure 2 a, b) are inside the hollow carbon spheres. The HCS surface was also seen to be rough and cratered. An EDX map showed that Ru is present in or on the hollow carbon spheres for both CoRu@HCS and Co@HCS@Ru (Figure S3). For the Co@HCS@Ru, the largest Ru peak has an intensity of ca. 1200 counts versus ca. 400 counts for the same peak for CoRu@HCS. Since the relative concentrations of Ru are similar in both samples the difference in peak heights for Ru (relative to Co) would indicate the presence of Ru outside the HCS for Co@HCS@Ru and inside the HCS for CoRu@HCS. On the Co@HCS@Ru catalyst, Co particles were located below the carbon shell surface while Ru particles are seen on the carbon surface, as shown on the secondary electron (SE) ~~image~~ in Figure 2 c, d. Furthermore, a combination of HAADF (transmission) and SE (surface) images clearly show that the small Ru nanoparticles are found on the outer carbon shell surface while the larger Co_3O_4 nanoparticles are below the carbon shell surface (as revealed by EDX) (Figure S.3).

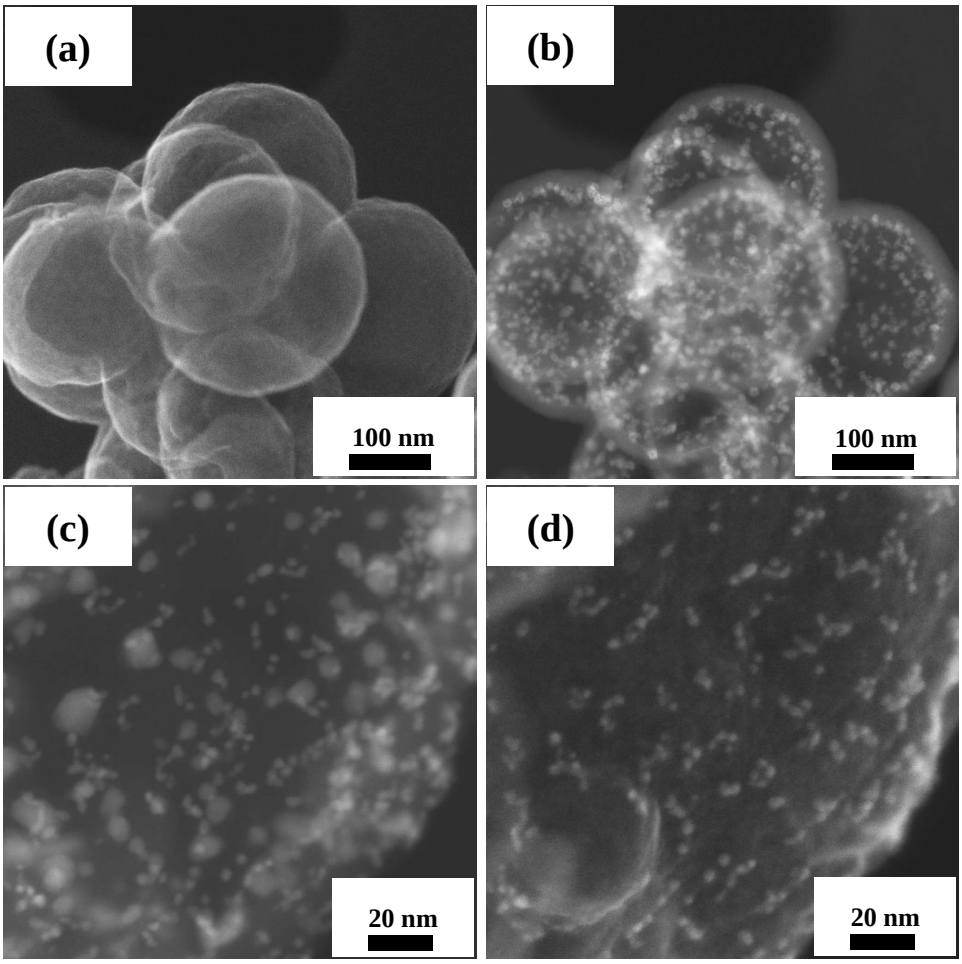

Figure 2: (a,b) SEM and STEM images of the same region of CoRu@HCS and (c,d) HAADF and secondary electron outer surface image of the same region of Co@HCS@Ru.

EDX line mapping (Figure S4) of a Co nanoparticle on Co@HCS@Ru revealed the presence of Co without any intimate contact between Co and Ru. However, a similar scan on the CoRu@HCS catalyst revealed the presence of Co and Ru at similar locations in the nanoparticle, thus suggesting that there is intimate contact between the two metals in this case. Using pair distribution function analysis and selected area electron diffraction of a highly magnified CoRu nanoparticle (Figure S5) evidence of Co-O, Co-Co and C-C bonds was observed; however evidence for a bimetallic Co-Ru bond was not observed **[29]**. This suggests that the Co and Ru nanoparticles in CoRu@HCS are in close physical contact but without forming chemical bonds between each other. However, only a few CoRu

nanoparticles were sampled by this method and the existence of a bimetallic CoRu particle in the catalyst cannot be completely ruled out.

Hydrogen pulse chemisorption experimental data was collected at 150 ℃ and is shown in Table 1. The dispersion for CoRu@HCS was more than double that of Co@HCS and Co@HCS@Ru. This can be attributed to the intimate contact of the Ru and Co atoms which enhanced the DOR of reduction on the Co nanoparticles without any sintering. The Ru promoter effects are more pronounced when the metal nanoparticles (i.e. Ru and Co) are near to one another and involve primary hydrogen spillover from the Ru to the Co_3O_4 nanoparticles. In contrast, the Co metallic dispersion in Co@HCS@Ru did not significantly vary from that of the unpromoted Co@HCS catalyst (0.007 versus 0.01). This indicates that Ru promoter effects through the carbon shell to the encapsulated Co_3O_4 nanoparticles were not as effective in enhancing the degree of reduction of the encapsulated nanoparticles. This suggests a more limited hydrogen spillover via a secondary process during the reaction conditions (note that the analysis temperature was 150 ℃ and the reduction temperature was 350 ℃).

Table 1: Co and Ru content, particle size and pulse chemisorption data of the catalyst composites.

Sample	Co dispersion (H:Co)[a]	Co_3O_4 particle size (nm)		Co_3O_4 and RuO_2 content (%) /TGA	Co loading (%)/ICP
		XRD[b]	TEM		
Co@HCS	0.007	6.1	7.4	12.5	9.1
Co@HCS@Ru	0.010	6.9	7.3	14.5	9.3
CoRu@HCS	0.028	6.2	7.1	14.0	9.0

[a]Obtained by pulse chemisorption, using a 1:1 ratio of hydrogen atoms to total moles of Co loaded on the sample. [b] Crystallite sizes estimated using Rietveld refinement.

TGA analysis (Figure 3a) under air revealed that all the catalysts had similar decomposition profiles. The onset of the carbon consumption via the oxidation step in which the carbon structure was converted to carbon dioxide occurred at approximately 310 ℃. Complete decomposition of the carbon in the catalysts was observed at temperatures between 550-620 ℃. The low decomposition temperature of these carbon materials is attributed to the catalytic effects of the metal nanoparticles on the carbon oxidation reaction, which have been observed in previous studies **[27, 30, 31]**. Hollow carbon spheres prepared from resorcinol formaldehyde as the carbon source contain defects and hence they are not highly thermally stable under an oxidizing environment. The residue for these catalysts (between 12-15%) was attributed to the cobalt oxide and ruthenium oxide particles, which allowed for an estimation of the loading of the metals in the three catalysts (Table 1 and Figure 3a). These loadings corresponded well with the metallic loadings that were obtained using ICP-OES analysis (Table 1).

Powder X-ray patterns confirmed the highly defective nature of the hollow carbon shells (i.e. no distinct carbon diffraction peaks), and that the encapsulated nanoparticles had the Co_3O_4 phase (ICSD collection number 9362), with the corresponding crystallite sizes as estimated by Rietveld refinement at 6.1, 6.9 and 6.2 nm for Co@HCS, Co@HCS@Ru and CoRu@HCS respectively. Raman spectroscopy (Figure S.6) also confirmed the presence of Co_3O_4 nanoparticles (i.e. A_{1g} band around 700 cm^{-1}) inside the hollow carbon spheres **[32, 33]**. The D and G bands of the carbon spheres also signified a carbon shell with significant defects as shown by the broadness of the D band peak and the D to G band intensity ratio (> 1), that indicates a highly defective carbon shell as suggested by the Robertson and Ferrari guidelines **[34, 35]**.

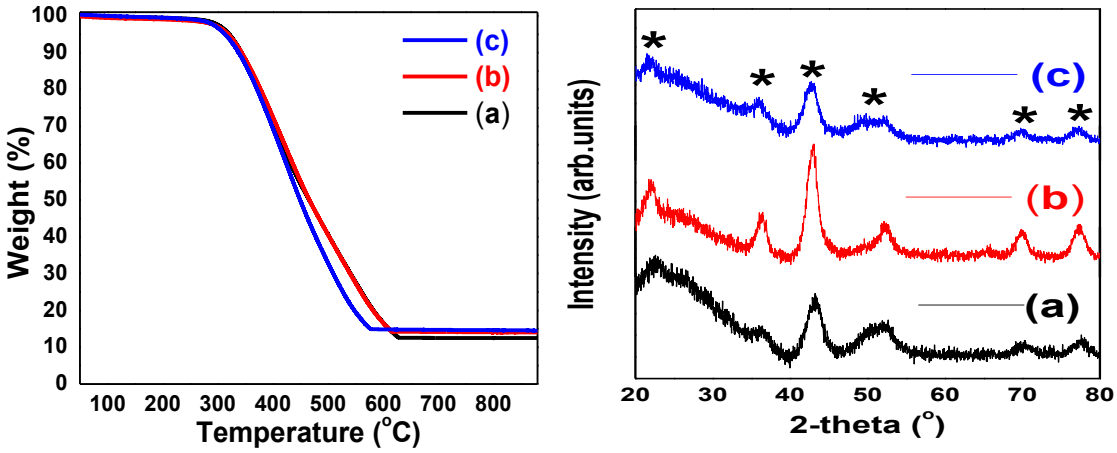

Figure 3. Thermogravimetric and PXRD data of (a) Co@HCS, (b) Co@HCS@Ru and (c) CoRu@HCS. (* indicates Co_3O_4 phase).

3.2. Carbon shell porosity

The adsorption isotherms of the three catalysts suggest that the carbon shell had a pore structure that is a type I/IV in nature (Figure 4) **[25]** containing both micropores and mesopores. This was supported by the high BET surface area between (440-480 m^2/g) and the fact that > 52 % of the total surface area on the catalysts was due to the microporous nature of the carbon shell (Table S.1). Empty HCS displayed a BET surface area of 465 m^2/g, within the same range thus implying that the encapsulation of Co nanoparticles did not alter the porosity of the carbon shell in the M@HCS materials. This microporosity was also confirmed by the pore size distribution plots, which showed significant nitrogen adsorption at average pore diameters of < 2 nm. Ideally, mesopores are the preferred pores because they allow for an easier diffusion as the high porosity allows for the easy diffusion of reactants and products both into and out of the hollow carbon sphere cavity **[11, 36]**.

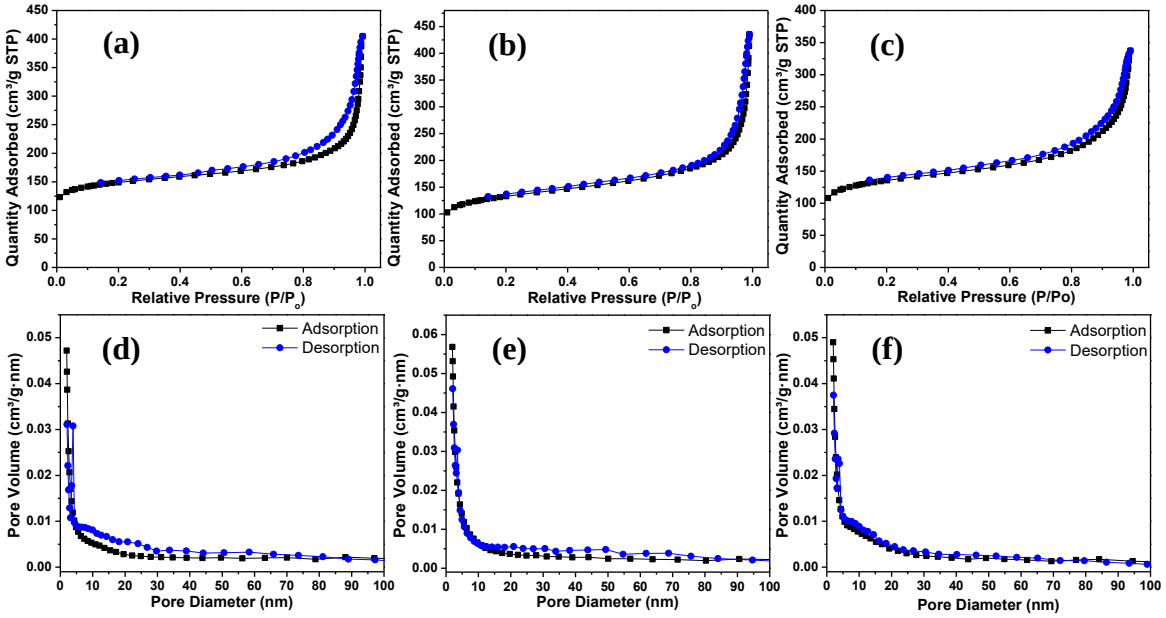

Figure 4. Nitrogen adsorption-desorption isotherms and pore size distribution plots of the catalysts. (a,d) Co@HCS, (b,e) CoRu@HCS and (c,f) Co@HCS@Ru.

3.3. Catalyst reduction using in situ PXRD

The reduction of the catalysts under hydrogen gas was studied by in situ PXRD at 50 ℃ intervals from 30 ℃ to 500 ℃ (Figure 5, Table S.3) **[37]**. Distinct reduction profiles were observed for the different catalysts. The Co@HCS catalyst displayed a phase transformation from Co_3O_4 to Co via the CoO intermediate. In the reduction, the cobalt oxide nanoparticles transformed to CoO at 250 ℃ while the transformation of CoO to fcc-Co began to be more pronounced at 300 ℃ and increased in intensity up to 500 ℃. However, the CoO was not completely reduced and appeared with the Co phase even at 500 ºC. In contrast, for Co@HCS@Ru complete Co_3O_4 conversion to CoO occurred at 250 ℃ (i.e., between 200 and 250 ℃), while the CoO phase transformation to fcc/hcp Co began at 350 ℃. A complete reduction of the CoO to Co was observed at 450 ℃. Both the fcc and hcp Co phases were observed, with the hcp Co phase being more pronounced indicating that the Ru metal promotion enhanced the formation of the hcp Co phase during activation by hydrogen reduction **[38]**.

The reduction of Co_3O_4 to CoO on CoRu@HCS was complete at 250 ℃ (similar to Co@HCS and Co@HCS@Ru). Further, a complete reduction to CoO to Co (fcc and hcp) appeared at 300 ℃, and from 350 ℃ to 500 ℃ the two Co phases were clearly observed in the diffraction patterns. The fcc phase was the dominant Co phase. The reduction profiles of the three catalysts for the conversion of Co_3O_4 to CoO are similar. This indicates that the Ru promoter regardless of its location relative to the Co_3O_4 did not significantly influence the hydrogen-induced conversion of $Co_3O_4$to CoO. However, the second reduction process, from CoO to Co, was visibly different for all the catalysts. These differences can be attributed to the location of the Ru promoter relative to that of the Co nanoparticles. The transformation temperature of CoO to Co increased: CoRu@HCS < Co@HCS@Ru < Co@HCS. This trend implies that when the Ru promoter was placed further away from the CoO nanoparticles the reduction temperature increased. The data confirms, as found in similar previous studies **[17]**, that when Co and Ru are separated by a carbon layer (as in Co@HCS@Ru) secondary hydrogen spillover processes can be detected.

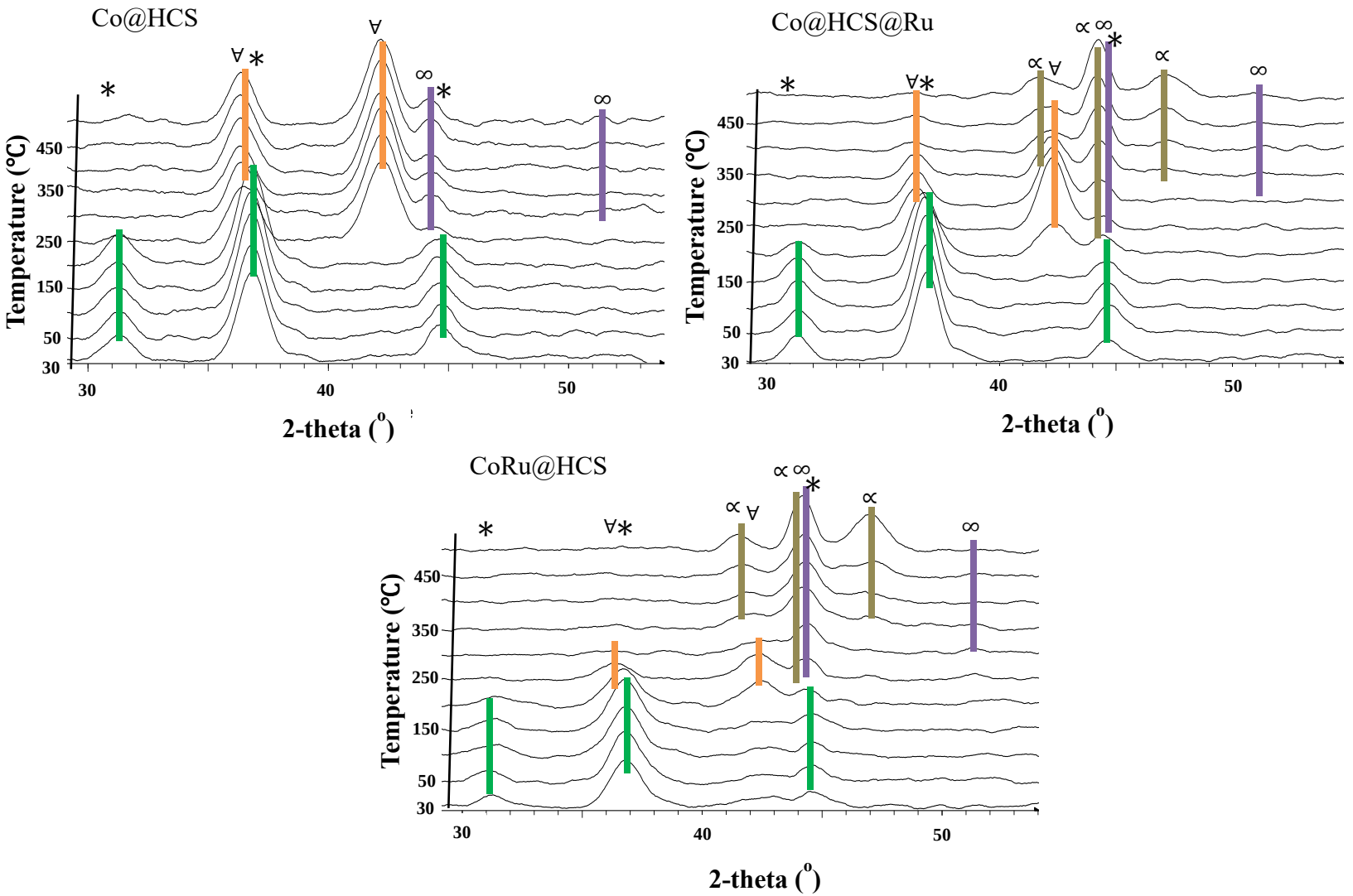

Figure 3: In situ PXRD profiles of the catalysts under reduction conditions. Co_3O_4 (*), CoO (∀), fcc-Co (∞), hcp-Co (α).

The degree of catalyst reduction was also evaluated from the in situ XRD patterns. This allowed a facile method to obtain the degree of reduction (DOR) at a specific temperature. Using the Rietveld refinement method, the DOR at 350 ℃ (the T used for the catalyst reduction) was approximately 29% for Co@HCS, 50% for Co@HCS@Ru, and 100% for CoRu@HCS (Figure 4). This can be compared to the actual DOR estimated by oxygen titration assuming a Co to Co_3O_4 transformation. The data, while lower at 21.5, 22.2 and 61.3% for Co@HCS, Co@HCS@Ru and CoRu@HCS respectively, showed similar trends to the one obtained from the XRD data (Figure S.7 and Table S.2) **[39]**.

The differences in the data can be attributed to the effect of the encapsulation of cobalt nanoparticles in the carbon nanoreactor. It is anticipated that some of the Co nanoparticle surfaces are not exposed to the oxygen gas as they were embedded inside the carbon shell microporous pore structure. An alternative and more likely explanation is that the formation of amorphous Co_xO_y phases cannot be detected during PXRD measurements [REF here]. This would enhance the DOR values from the Rietveld refinement calculations as compared to those from oxygen titration values **[37, 40].** Nonetheless, the observed DOR trends on these catalysts suggest a location-dependent effect of the Ru metal toward reduction of cobalt oxide nanoparticles due to the carbon shell barrier.

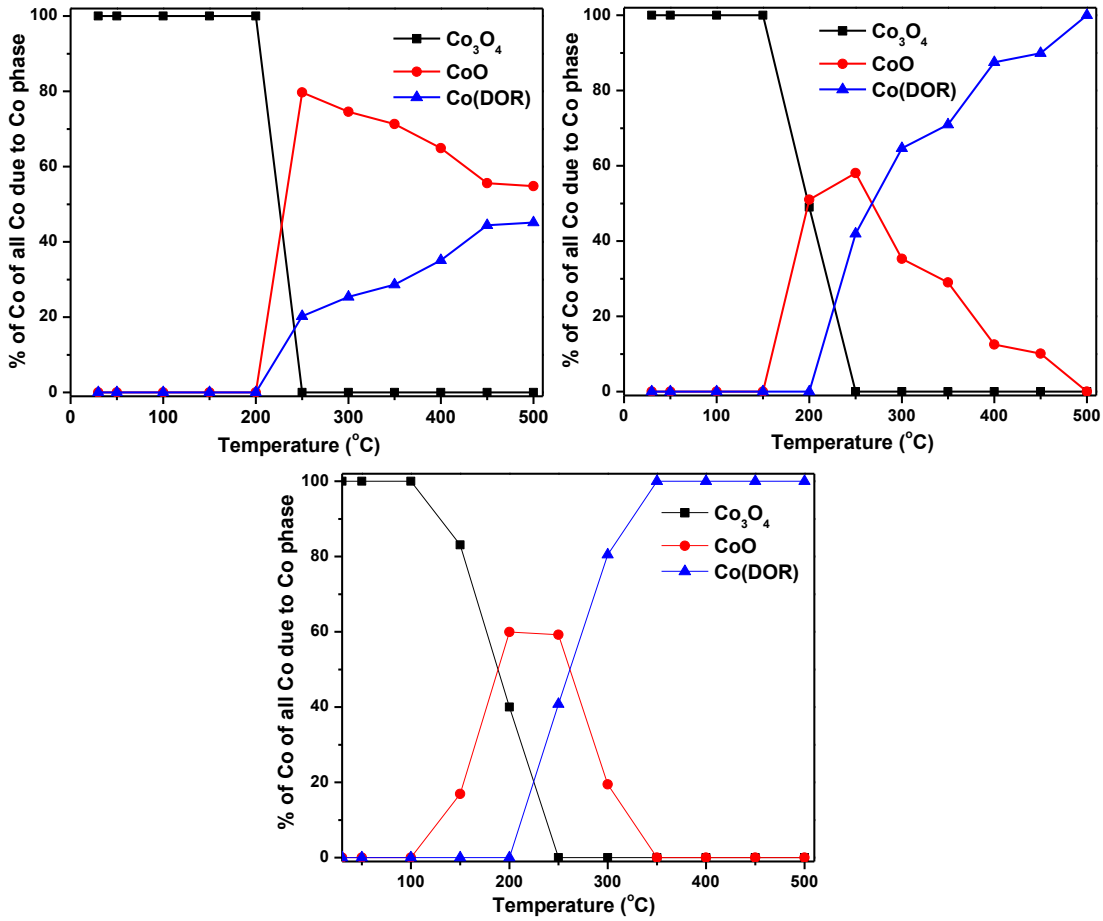

Figure 4: Co phase abundance changes as a function of temperature during in situ PXRD under a hydrogen environment: (a) Co@HCS, (b) Co@HCS@Ru, (c) CoRu@HCS.

The in situ PXRD studies indicate that both primary and secondary hydrogen spillover processes can be observed for these Ru promoted Co catalysts. It should, however, be noted that based on the observed reduction temperatures (specifically for the CoO to Co transformation) that the primary spillover is favored over secondary hydrogen spillover due to the surface diffusion of hydrogen on the carbon support being a rate-limiting step **[19]**.

Reduction analysis using temperature programmed reduction (Figure S8, Table S4) is consistent with the in situ XRD studies. Similar reduction profiles for the Co@HCS and Co@HCS@Ru, with the Co_3O_4 to CoO transformation, occurred at 323 and 312 ℃ and the

CoO to Co phase transformation occurred at 415 and 414 ℃ respectively. However, the CoRu@HCS catalyst had a much lower reduction temperature (264 ℃) **[41]**. From the TPR data, it can be concluded that the effect of Ru nanoparticles on the Co oxide nanoparticle reduction could not be effectively detected and separated with respect to the unpromoted Co@HCS. This could be linked to the gasification of carbon support at higher temperatures to form methane whose TCD signal overlaps with the signals that correspond to the hydrogen consumption by the Co oxide phases. The carbon support gasification (see Figure S8 and Table S4; peak at approximately 700 ℃) was substantial on these catalysts due to the high defect content and low graphitic nature of these hollow carbon spheres.

3.4. Fischer-Tropsch (FT) synthesis

The FT evaluation of the catalysts was performed at 220 ℃ and 10 bar pressure (Table 2 and Figure S9 &S10) after activation in a hydrogen atmosphere at 350 ℃. In this study, the catalysts are confined in the HCS which can be regarded as nanoreactors. Diffusional issues are thus expected, especially for the high molecular weight carbons produced in the reaction. To limit this issue, conditions were chosen to limit carbon polymerization. Notwithstanding this, the TOF is low compared to other catalysts reported in the literature and can be attributed to the microporous nature of the hollow carbon spheres that leads to diffusion limitations for reactant and the products **[11, 36]**.

However, it is clear that FT synthesis did occur and this indicates that FT reactions can be performed inside carbon nanoreactors.

In this study, catalyst activity correlated with the catalysts's DOR, with CO conversion of 11.8, 12.4, 18.3% were observed for Co@HCS, Co@HCS@Ru, and CoRu@HCS respectively. The catalyst turnover frequency increased with the increasing intimacy of the Co and Ru metals (from 14 to 24 $\times 10^{-4}$ s^{-1}). This is consistent with literature reports where it has been shown that by loading the Co and Ru metals using a co-precipitation method or a sequential method, the Co and Ru had different contact distances and that this affected Fischer-Tropsch activities, that changed with the Co-Ru contact **[41-43]**. Here the impact of a primary spillover effect due to the HCS support can be seen (compare Co@HCS and CoRu@HCS).

Although the high degree of reduction on CoRu@HCS due to the primary hydrogen spillover should also lead to high Fischer-Tropsch activity, as evidenced by the Fischer-Tropsch data, a synergistic effect on the Ru promoted Co catalyst cannot also be ruled out to explain the observed data. This is due to the positive electronic effects that a Ru promoter affords to Co atoms and their corresponding nanoparticles as it relates to its enhanced ability to dissociate hydrogen and carbon monoxide at higher rates **[41, 43].**

Nonetheless, the Ru did not dramatically enhance the Co activity and degree of reduction on Co@HCS@Ru. It can thus be concluded that the secondary hydrogen spillover process did not significantly assist in increasing the Fischer-Tropsch activity, possibly due to the decreased diffusion rate of the spillover hydrogen at the reaction temperature (i.e. 220 ℃) and the reduction conditions used (at 350 ℃). Therefore, only a limited effect of the Ru promoter on the Fischer-Tropsch activity of Co in the Co@HCS@Ru catalyst was observed, when compared with the unpromoted Co@HCS.

Table 2. Fischer-Tropsch Synthesis results.

Sample	CO Conversion (%)	Activity $\times 10^{-6}$ ($mol_{CO}/g_{Co}.s$)	TOF (s^{-1} 10^{-4})	Selectivity (C mol) %		
				C_1	C_2-C_4	C_{5+}
Co@HCS	11.8	3.64	14	19	10	71
Co@HCS@Ru	12.4	4.68	18	21	8	71
CoRu@HCS	18.3	6.07	24	37	14	49

Sample	Olefinicity (%)			
	α	C_2	C_3	C_4
Co@HCS	0.74	21.2	200	129
Co@HCS@Ru	0.69	5.6	96	60
CoRu@HCS	0.61	6.8	115	68

Hydrocarbon selectivity (Table 2 and Figure S10) for the catalysts suggests that the Ru promoter in these studies increased the formation of methane and paraffins. Methane

selectivity increased as the Ru and Co nanoparticles intimacy increased; 19, 21 and 37% for Co@HCS, Co@HCS@Ru, and CoRu@HCS. Numerous studies have shown that the hydrogen dissociation on noble metal promoters of Co FT catalysts gives a product distribution with high methane selectivity **[22, 44, 45].** The high methane selectivity is however in contrast with several other studies where Co catalysts were promoted by Ru **[46, 47]**. In our study, the high methane selectivity can also be attributed to the microporosity of the nanoreactors that held up the high molecular weight products leading to their slow rate of effusion. High methane selectivity invariably leads to decreasing C_{5+} selectivity (71% for Co@HCS, 71% for Co@HCS@Ru and 49% for CoRu@HCS), this also corresponded to the decreased ASF values of 0.74, 0.69 and 0.61 respectively. Catalyst olefinicity was evaluated using the C_2-C_4 products. The presence of the Ru promoter enhanced the formation of alkanes over alkenes (see Table 2). The olefinicity of Co@HCS@Ru and CoRu@HCS was low as compared to the Co@HCS catalyst. The lowering of the olefin content in the product spectrum was attributed to the Ru promoter and its high propensity to dissociate hydrogen - hence the high hydrogen concentration on the catalyst surfaces increased the hydrogenation rate of the olefins **[22, 43].**

4. Conclusion

We report on the synthesis of a catalytic nanoreactor for application in the Fischer-Tropsch Synthesis using cobalt nanoparticles encapsulated inside hollow carbon spheres. This synthetic method yielded porous catalyst composites whose morphology and defective nature was also exploited to study the effect of hydrogen spillover in the Fischer-Tropsch process. Co and CoRu nanoparticles with similar particle sizes were successfully encapsulated inside mesoporous hollow carbon spheres, while the third catalyst was prepared by loading Ru nanoparticles on the outside of Co@HCS catalysts. This gave catalysts with Co and Ru separated by the HCS support. The catalyst reducibility (determined by in situ PXRD) was in the order CoRu@HCS > Co@HCS@Ru > Co@HCS and suggests that both primary and secondary spillover effects were observed leading to enhanced Co_3O_4 reduction.

The Fischer-Tropsch reaction results suggest that the HCS can act as a nanoreactor in FT synthesis reactions. Highly hydrogenated products were formed due to the presence of the Ru promoter, owing to the hydrogen-enriched surfaces due to the hydrogen spillover. On the

carbon support, secondary hydrogen spillover did not appear to enhance the catalyst activity of Co@HCS@Ru when compared to the unpromoted Co@HCS catalyst.

Acknowledgements

We wish to thank the DST-NRF Centre of Excellence in Catalysis, the NRF and the University of the Witwatersrand for financial assistance. We also acknowledge Johnson-Matthey for collecting the STEM/EDAX data on the catalysts

References

1. Lee J, Kim SM, Lee IS: **Functionalization of hollow nanoparticles for nanoreactor applications**. *Nano Today* 2014, **9**(5):631-667.
2. Shi R, Wang J, Zhao J, Liu S, Hao P, Li Z, Ren J: **Cu nanoparticles encapsulated with hollow carbon spheres for methanol oxidative carbonylation: Tuning of the catalytic properties by particle size control**. *Applied Surface Science* 2018, **459**:707-715.
3. Tan H, Li Y, Kim J, Takei T, Wang Z, Xu X, Wang J, Bando Y, Kang YM, Tang J: **Sub-50 nm Iron–Nitrogen-Doped Hollow Carbon Sphere-Encapsulated Iron Carbide Nanoparticles as Efficient Oxygen Reduction Catalysts**. *Advanced Science* 2018, **5**(7):1800120.
4. Fang X, Zhao X, Fang W, Chen C, Zheng N: **Self-templating synthesis of hollow mesoporous silica and their applications in catalysis and drug delivery**. *Nanoscale* 2013, **5**(6):2205-2218.
5. Song X, Gao L: **Synthesis, characterization, and optical properties of well-defined N-doped, hollow silica/titania hybrid microspheres**. *Langmuir* 2007, **23**(23):11850-11856.
6. Chen X, Kierzek K, Wenelska K, Cendrowski K, Gong J, Wen X, Tang T, Chu PK, Mijowska E: **Electrochemical Characteristics of Discrete, Uniform, and Monodispersed Hollow Mesoporous Carbon Spheres in Double-Layered Supercapacitors**. *Chemistry–An Asian Journal* 2013, **8**(11):2627-2633.

7. Liu T, Zhang L, Cheng B, Yu J: **Hollow Carbon Spheres and Their Hybrid Nanomaterials in Electrochemical Energy Storage**. *Advanced Energy Materials* 2019:1803900.
8. Dlamini MW, Phaahlamohlaka TN, Kumi DO, Forbes R, Jewell LL, Coville NJ: **Post doped nitrogen-decorated hollow carbon spheres as a support for Co Fischer-Tropsch catalysts**. *Catalysis Today* 2019.
9. Zhang C, Zhang R, Gao X, Cheng C, Hou L, Li X, Chen W: **Small naked Pt nanoparticles confined in mesoporous shell of hollow carbon spheres for high-performance nonenzymatic sensing of H2O2 and glucose**. *Acs Omega* 2018, **3**(1):96-105.
10. Ikeda S, Ishino S, Harada T, Okamoto N, Sakata T, Mori H, Kuwabata S, Torimoto T, Matsumura M: **Ligand-Free Platinum Nanoparticles Encapsulated in a Hollow Porous Carbon Shell as a Highly Active Heterogeneous Hydrogenation Catalyst**. *Angewandte Chemie* 2006, **118**(42):7221-7224.
11. Nongwe I, Bepete G, Shaikjee A, Ravat V, Terfassa B, Meijboom R, Coville NJ: **Synthesis of gold encapsulated in spherical carbon capsules with a mesoporous shell structure. A robust catalyst in a nanoreactor**. *Catalysis Communications* 2014, **53**:77-82.
12. Bian S-W, Liu S, Guo M-X, Xu L-L, Chang L: **Pd nanoparticles partially embedded in the inner wall of nitrogen-doped carbon hollow spheres as nanoreactors for catalytic reduction of 4-nitrophenol**. *RSC Advances* 2015, **5**(16):11913-11916.
13. Harada T, Ikeda S, Ng YH, Sakata T, Mori H, Torimoto T, Matsumura M: **Rhodium nanoparticle encapsulated in a porous carbon shell as an active heterogeneous catalyst for aromatic hydrogenation**. *Advanced Functional Materials* 2008, **18**(15):2190-2196.
14. White RJ, Tauer K, Antonietti M, Titirici M-M: **Functional hollow carbon nanospheres by latex templating**. *Journal of the American Chemical Society* 2010, **132**(49):17360-17363.

15. Gorsd MN, Blanco MN, Pizzio LR: **Synthesis of polystyrene microspheres to be used as template in the preparation of hollow spherical materials: study of the operative variables**. *Procedia Materials Science* 2012, **1**:432-438.
16. Phaahlamohlaka TN, Dlamini MW, Mogodi MW, Kumi DO, Jewell LL, Billing DG, Coville NJ: **A sinter resistant Co Fischer-Tropsch catalyst promoted with Ru and supported on titania encapsulated by mesoporous silica**. *Applied Catalysis A: General* 2018, **552**:129-137.
17. Phaahlamohlaka TN, Kumi DO, Dlamini MW, Forbes R, Jewell LL, Billing DG, Coville NJ: **Effects of Co and Ru Intimacy in Fischer–Tropsch Catalysts Using Hollow Carbon Sphere Supports: Assessment of the Hydrogen Spillover Processes**. *ACS Catalysis* 2017, **7**(3):1568-1578.
18. Vosoughi V, Dalai AK, Abatzoglou N, Hu Y: **Performances of promoted cobalt catalysts supported on mesoporous alumina for Fischer-Tropsch synthesis**. *Applied Catalysis A: General* 2017, **547**:155-163.
19. Beaumont SK, Alayoglu S, Specht C, Kruse N, Somorjai GA: **A nanoscale demonstration of hydrogen atom spillover and surface diffusion across silica using the kinetics of CO2 methanation catalyzed on spatially separate Pt and Co nanoparticles**. *Nano letters* 2014, **14**(8):4792-4796.
20. Sermon P, Bond G: **Hydrogen spillover**. *Catalysis Reviews* 1974, **8**(1):211-239.
21. Karim W, Spreafico C, Kleibert A, Gobrecht J, VandeVondele J, Ekinci Y, van Bokhoven JA: **Catalyst support effects on hydrogen spillover**. *Nature* 2017, **541**(7635):68.
22. Nabaho D, Niemantsverdriet JH, Claeys M, Van Steen E: **Hydrogen spillover in the Fischer–Tropsch synthesis: An analysis of platinum as a promoter for cobalt–alumina catalysts**. *Catalysis Today* 2016, **261**:17-27.
23. Prins R: **Hydrogen spillover. Facts and fiction**. *Chemical reviews* 2012, **112**(5):2714-2738.
24. Chen Y, Liew KY, Li J: **Size-controlled synthesis of Ru nanoparticles by ethylene glycol reduction**. *Materials Letters* 2008, **62**(6-7):1018-1021.
25. Gregg SJ, Sing KSW, Salzberg H: **Adsorption surface area and porosity**. *Journal of The Electrochemical Society* 1967, **114**(11):279C-279C.

26. Barrett EP, Joyner LG, Halenda PP: **The determination of pore volume and area distributions in porous substances. I. Computations from nitrogen isotherms**. *Journal of the American Chemical society* 1951, **73**(1):373-380.
27. Phaahlamohlaka TN, Kumi DO, Dlamini MW, Forbes R, Jewell LL, Billing DG, Coville NJ: **Effects of Co and Ru intimacy in Fischer-Tropsch catalysts using hollow carbon sphere supports: assessment of the hydrogen spillover processes**. *ACS Catalysis* 2016.
28. Qiao Z-A, Guo B, Binder AJ, Chen J, Veith GM, Dai S: **Controlled synthesis of mesoporous carbon nanostructures via a "silica-assisted" strategy**. *Nano letters* 2012, **13**(1):207-212.
29. Mu X, Wang D, Feng T, Kübel C: **Radial distribution function imaging by STEM diffraction: Phase mapping and analysis of heterogeneous nanostructured glasses**. *Ultramicroscopy* 2016, **168**:1-6.
30. Dlamini MW, Kumi DO, Phaahlamohlaka TN, Lyadov AS, Billing DG, Jewell LL, Coville NJ: **Carbon spheres prepared by hydrothermal synthesis—a support for bimetallic iron cobalt Fischer–Tropsch catalysts**. *ChemCatChem* 2015, **7**(18):3000-3011.
31. Xiong H, Moyo M, Motchelaho MA, Tetana ZN, Dube SM, Jewell LL, Coville NJ: **Fischer–Tropsch synthesis: Iron catalysts supported on N-doped carbon spheres prepared by chemical vapor deposition and hydrothermal approaches**. *Journal of Catalysis* 2014, **311**:80-87.
32. Tang C-W, Wang C-B, Chien S-H: **Characterization of cobalt oxides studied by FT-IR, Raman, TPR and TG-MS**. *Thermochimica Acta* 2008, **473**(1):68-73.
33. Hadjiev V, Iliev M, Vergilov I: **The Raman spectra of Co3O4**. *Journal of Physics C: Solid State Physics* 1988, **21**(7):L199.
34. Ilie A, Hart A, Flewitt A, Robertson J, Milne W: **Effect of work function and surface microstructure on field emission of tetrahedral amorphous carbon**. *Journal of Applied Physics* 2000, **88**(10):6002-6010.
35. Ferrari AC, Robertson J: **Interpretation of Raman spectra of disordered and amorphous carbon**. *Physical review B* 2000, **61**(20):14095.

36. Phaahlamohlaka TN, Kumi DO, Dlamini MW, Jewell LL, Coville NJ: **Ruthenium nanoparticles encapsulated inside porous hollow carbon spheres: A novel catalyst for Fischer–Tropsch synthesis**. *Catalysis Today* 2016, **275**:76-83.
37. Rayner MK, Billing DG, Coville NJ: **In-situ X-ray diffraction activation study on an Fe/TiO2 pre-catalyst**. *Acta Crystallographica Section B: Structural Science, Crystal Engineering and Materials* 2014, **70**(3):498-509.
38. Liu J-X, Su H-Y, Sun D-P, Zhang B-Y, Li W-X: **Crystallographic dependence of CO activation on cobalt catalysts: HCP versus FCC**. *Journal of the American Chemical Society* 2013, **135**(44):16284-16287.
39. Li J, Coville NJ: **The effect of boron on the catalyst reducibility and activity of Co/TiO 2 Fischer–Tropsch catalysts**. *Applied Catalysis A: General* 1999, **181**(1):201-208.
40. du Plessis HE, Forbes RP, Barnard W, Erasmus WJ, Steuwer A: **In situ reduction study of cobalt model Fischer–Tropsch synthesis catalysts**. *Physical Chemistry Chemical Physics* 2013, **15**(28):11640-11645.
41. Hong J, Marceau E, Khodakov AY, Gaberová L, Griboval-Constant A, Girardon J-S, Fontaine CL, Briois V: **Speciation of ruthenium as a reduction promoter of silica-supported Co catalysts: a time-resolved in situ XAS investigation**. *ACS Catalysis* 2015, **5**(2):1273-1282.
42. Cook KM, Perez HD, Bartholomew CH, Hecker WC: **Effect of promoter deposition order on platinum-, ruthenium-, or rhenium-promoted cobalt Fischer–Tropsch catalysts**. *Applied Catalysis A: General* 2014, **482**:275-286.
43. Iglesia E, Soled SL, Fiato RA, Via GH: **Bimetallic synergy in cobalt ruthenium Fischer-Tropsch synthesis catalysts**. *Journal of Catalysis* 1993, **143**(2):345-368.
44. Kogelbauer A, Goodwin Jr JG, Oukaci R: **Ruthenium Promotion of Co/Al2O3Fischer–Tropsch Catalysts**. *Journal of Catalysis* 1996, **160**(1):125-133.
45. Nabaho D, Niemantsverdriet JH, Claeys M, van Steen E: **Hydrogen spillover in the Fischer–Tropsch synthesis: An analysis of gold as a promoter for cobalt–alumina catalysts**. *Catalysis Today* 2016, **275**:27-34.

46. Xu D, Li W, Duan H, Ge Q, Xu H: **Reaction performance and characterization of Co/Al 2 O 3 Fischer–Tropsch catalysts promoted with Pt, Pd and Ru**. *Catalysis Letters* 2005, **102**(3):229-235.

47. Hong J, Chernavskii PA, Khodakov AY, Chu W: **Effect of promotion with ruthenium on the structure and catalytic performance of mesoporous silica (smaller and larger pore) supported cobalt Fischer–Tropsch catalysts**. *Catalysis Today* 2009, **140**(3):135-141.

List of Tables

Table 1: Co and Ru content, particle size and pulse chemisorption data of the catalyst composites.

Table 2: Fischer-Tropsch Synthesis results.

List of Figures

Figure 1: TEM images and particle size distribution of the prepared catalysts together with the presynthesized Ru nanoparticles. (a,b) Co@HCS (c,d) CoRu@HCS, (e,f) Ru

Figure 2: (a,b) SEM and STEM images of the same region of CoRu@HCS and (c,d) HAADF and secondary electron outer surface image of the same region of Co@HCS@Ru.

Figure 3: (a) Thermogravimetric and (b) PXRD diffraction data of the catalyst materials, (*) Co_3O_4.

Figure 4: Nitrogen adsorption-desorption isotherms and pore size distribution plots of the catalysts. (a,d) Co@HCS, (b,e) CoRu@HCS and (c,f) Co@HCS@Ru.

Figure 5: In situ PXRD profiles of the catalysts under reduction conditions. Co_3O_4 (*), CoO (∀), α-Co (∞), β-Co (α).

Figure 6: Co phase abundance changes as a function of temperature during in situ PXRD under a hydrogen environment: (a) Co@HCS, (b)Co@HCS@Ru, (c) CoRu@HCS.